CrossMark

Solar Models with Dynamic Screening and Early Mass Loss Tested by Helioseismic, Astrophysical, and Planetary Constraints

Suzannah R. Wood[1] (ID) · **Katie Mussack**[1] (ID) ·
Joyce A. Guzik[2] (ID)

Abstract The faint young Sun paradox remains an open question. Presented here is one possible solution to this apparent inconsistency, a more massive early Sun. Based on the conditions on early Earth and Mars, a luminosity constraint is set as a function of mass. We examine helioseismic constraints of these alternative mass-losing models. Additionally, we explore a dynamic electron screening correction in an effort to improve helioseismic agreement in the core of the early mass-losing model.

Keywords Oscillations · Solar

1. Introduction

There is evidence for the presence of liquid water on Earth as early as 4.3 Gyrs ago, and on Mars as early 3.8 Gyrs ago. However, for 1 $M_\odot$ standard solar evolution modes, the solar luminosity was 70% of the current solar luminosity at the beginning of the Sun's main-sequence lifetime, which is not enough for the presence of liquid water at these early times. This inconsistency is known as the "faint young Sun paradox." There have been proposed many ways to account for this apparent contradiction (*e.g.*, greenhouse gases effects (Forget *et al.*, 2013; Turbet *et al.*, 2017; Bristow *et al.*, 2017; Wordsworth, 2016), carbon cycle (Charnay *et al.*, 2017), coronal mass ejections (Airapetian *et al.*, 2016), and more massive early Sun (Sackmann and Boothroyd, 2003; Minton and Malhotra, 2007; Turck-Chièze, Piau, and Couvidat, 2011; Weiss and Heners, 2013)).

✉ S.R. Wood
suzannah@lanl.gov

K. Mussack
mussack@lanl.gov

J.A. Guzik
joy@lanl.gov

1   Los Alamos National Laboratory, XTD-IDA, MS T-086, Los Alamos, NM 87545, USA

2   Los Alamos National Laboratory, XTD-NTA, MS T-082, Los Alamos, NM 87545, USA

It is possible that the higher mass-loss rates seen in pre-main-sequence stars extend into the early main sequence, and it is reasonable to assume that the mass-loss rate decreases rather quickly with time on the main sequence (*e.g.*, power law or exponentially as used by *e.g.*, Wood *et al.*, 2002, 2005b,a; Ribas, 2010; Guzik, Willson, and Brunish, 1987). Therefore, the Sun could have begun its main-sequence evolution at higher mass and luminosity (as investigated by *e.g.*, Guzik, Willson, and Brunish, 1987; Turck-Chieze, Daeppen, and Casse, 1988; Sackmann and Boothroyd, 2003; Minton and Malhotra, 2007; Turck-Chièze, Piau, and Couvidat, 2011; Weiss and Heners, 2013).

Here, we use the solar luminosity requirement suggested by the presence of liquid water on early Earth and Mars to place limits on the initial mass of a more massive, luminous Sun, assuming an exponentially decaying mass-loss rate. We examine the interior sound speed and oscillation frequencies of these alternate solar models and compare with helioseismic constraints.

As found by Guzik and Mussack (2010), early mass loss can improve the sound-speed agreement with helioseismic inferences in the radiative interior outside the core H-burning region, but worsens the agreement in the solar core. Mussack and Däppen (2011) found that taking into account electron screening corrections to nuclear reaction rates based on molecular dynamics simulations resulted in a change in core sound speed in the opposite direction to the effects of early mass loss. Here we investigate the compensating effects on the core structure of including both early mass-loss and dynamical electron screening corrections simultaneously.

2. Solar Evolution Models

The Los Alamos group models use a one-dimensional evolution code updated from the Iben (1963, 1965a,b) code. Updates to the Iben (1963, 1965a,b) code, are the same changes as implemented in Guzik and Mussack (2010). These include use of the OPAL opacities (Iglesias and Rogers, 1996) supplemented by the Ferguson *et al.* (2005) or Alexander and Ferguson (private communication, 1995) low-temperature opacities, SIREFF equation of state (see Guzik and Swenson, 1997), Burgers' diffusion treatment (for implementation see Cox, Guzik, and Kidman, 1989), and nuclear reaction rates from NACRE (Angulo *et al.*, 1999), with a correction to the ^{14}N rate from Formicola *et al.* (2004). In this work the abundances of Asplund, Grevesse, and Sauval (2005) and Grevesse and Noels (1993) will be employed to bracket the range of abundance determinations.

For a full description of the physics, data, and codes used in the models discussed here, refer to Guzik and Mussack (2010) and Guzik, Watson, and Cox (2005). For a description of the mass-loss function, refer to Guzik, Willson, and Brunish (1987).

Models were computed from the pre-main-sequence contraction phase, when the luminosity generated from gravitational contraction exceeded the luminosity generated by nuclear reactions by a factor of several times, through the present day. For mass-loss models, the model was evolved at a constant mass until the zero-age main sequence, defined as a minimum in radius, at which point the mass loss was turned on. The evolution models were adjusted to present standard solar values within uncertainties: present solar age (4.54 ± 0.04 Gyr, Guenther *et al.*, 1992), radius (6.9599×10^{10} cm, Allen, 1973), mass (1.989×10^{33} g, Cohen and Taylor, 1988), luminosity (3.846×10^{33} erg/g, Willson *et al.*, 1986), and specified photospheric ratio (Z/X). This was done by modifying the initial heavy element mass fraction (Z), initial helium mass fraction (Y), and the mixing length

Table 1 Initial conditions (mass, abundances), mixing-length parameter, and final conditions (abundances, CZ base).

Model	$M_o/M_\odot$	Y_o	Z_o	α	Z/X	Y_{CZ}[a]	$R_{CZB}/R_\odot$[b]
GN93	1.00	0.2693	0.0196	2.0324	0.0239	0.2414	0.7185
AGS05	1.00	0.2570	0.0135	1.9832	0.0163	0.2272	0.7307
ML107	1.07	0.2545	0.0135	1.9912	0.0169	0.2393	0.7295
ML115	1.15	0.2528	0.0135	2.0104	0.0172	0.2348	0.7258
ML130	1.30	0.2466	0.0135	2.0571	0.0178	0.2388	0.7217
AGSpp0	1.00	0.2576	0.0135	2.0139	0.0158	0.2277	0.7296
ML107pp0	1.07	0.2550	0.0135	1.9710	0.169	0.2359	0.7334
ML130rx0	1.30	0.2476	0.0135	2.0302	0.0167	0.2291	0.7257

[a]Seismically inferred values from Basu and Antia (2004): $Y_{CZ} = 0.2485 \pm 0.0035$.

[b]Seismically inferred values from Basu and Antia (2004): $R_{CZB}/R_\odot = 0.713 \pm 0.001$.

to pressure-scale height-ratio (α); see Table 1 for initial and final values as regards our models.

The mass-loss function decays exponentially with an e-folding time of 0.45 Gyr. This simple mass-loss treatment is smooth, decreases with time, and most of the mass is lost at early times. This mass-loss treatment was chosen because low-mass stars (like solar-mass stars) lose angular momentum quickly during main-sequence evolution (Wolff and Simon, 1997) via magnetized stellar winds (Schatzman, 1962; Weber and Davis, 1967), due to a lower specific angular momentum. This mass loss occurs predominantly in the early lifetime of the star at ages less than 1 Gyr, for solar-like stars (Gallet and Bouvier, 2013). The present solar mass-loss rate does not affect the Sun's evolution (2×10^{-14} $M_\odot$ Feldman *et al.*, 1977).

The dynamic electron screening correction was implemented following the treatment of Mussack and Däppen (2011).

3. Results and Discussion

3.1. Determining Luminosity Constraints Based on Planetary Conditions

By examining the conditions on the planets at early times, useful constraints can be placed on the early-time luminosity of the Sun. Conditions on the early Earth can be used as an upper constraint on luminosity, while those on early Mars can be used as lower constraint on luminosity based on their relative positions to the Sun. According to the standard solar model, the Earth should have been too cold for liquid water for the entire Archaean period, approximately the first half of its existence (Kasting, 2010); however, it was not.

The first evidence of a hydrosphere interacting with the Earth's crust was from 4300 million years ago ($t = 0.24$ Gyrs) (Mojzsis, Harrison, and Pidgeon, 2001). This suggests that the luminosity of the Sun needed to be low enough at this time to prevent the photodissociation of water and subsequent loss of H_2 into space. Whitmire *et al.* (1995) provides constraints on mass loss based on the flux that reaches Earth at a given solar age. According to Kasting (1988) this would occur if the flux experienced by early Earth exceeds 1.1 $F_\odot$. If the average distance between the Earth and the Sun is assumed to be the same today as it was early in the Sun's evolution, then the Sun's maximum luminosity at early times could
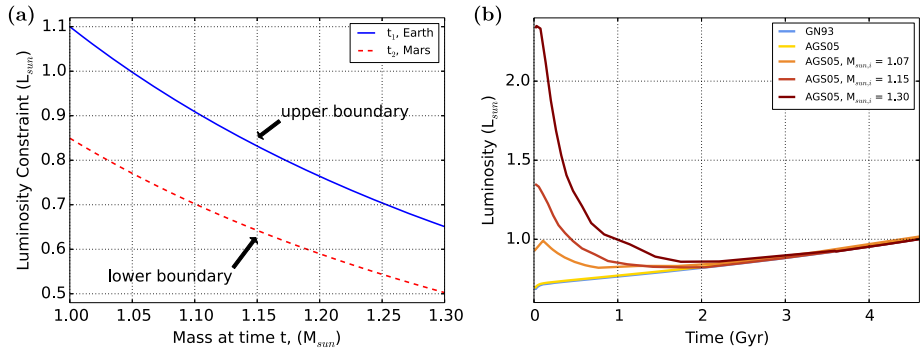
Figure 1 (**a**) Planetary constraints on luminosity as a function of solar mass at time (t). Photodissociation of water from Earth at $t_1 = 0.24$ Gyr is *blue*. Freezing of water on Mars at $t_2 = 0.74$ Gyr is *red*. (**b**) Luminosity *versus* time for solar models. Models include: standard solar models with GN93 (*blue*) and AGS05 (*yellow*) abundances, and early mass-losing models using the AGS05 abundances and initial masses of 1.07, 1.15 and 1.30 $M_\odot$ (*orange to maroon* with increasing initial mass).

not exceed 1.1 $L_\odot$. However, if we were to consider a more massive Sun to explain the "faint young Sun paradox," the distance between the early Earth and the early Sun would change as a function of the solar mass; therefore the luminosity to maintain liquid water on Earth would change as a function of mass. Even though the Earth's eccentricity varies by up to 6% during the 100,000 year Milankovitch cycle, we assumed that the eccentricity of the Earth's orbit and the angular momentum per unit mass of the Earth remain constant with time, the average distance between the Earth and the Sun would be inversely proportional to the $M_\odot(t)$ at time t. Based on the condition that the flux experienced by early Earth does not exceed 1.1 $F_\odot$, Figure 1(a) shows how the corresponding constraint on the luminosity varies with solar mass. The blue line shows the upper limit on the solar luminosity at $t_1 = 0.24$ Gyr.

In addition, there is substantial geomorphological and geochemical evidence for liquid water on Mars at the end of the late bombardment period (Carr, 1996; Malin and Edgett, 2000, 2003; Ehlmann *et al.*, 2008; Boynton *et al.*, 2009; Morris *et al.*, 2010; Osterloo *et al.*, 2008; Lanza *et al.*, 2016; Poulet *et al.*, 2005; Bibring *et al.*, 2006; Ehlmann *et al.*, 2011; Gendrin *et al.*, 2005; Squyres *et al.*, 2004, 2008; Bristow *et al.*, 2017; Turbet *et al.*, 2017). In fact, Kasting (1991) and Kasting, Whitmire, and Reynolds (1993) suggested that the solar flux needed to be 13% greater than predicted by the standard solar model at the end of the late heavy bombardment period (3.8 Gyr ago, $t_2 = 0.74$ Gyr) in order for Mars to be warm enough for liquid water. However, if we were to consider a more massive Sun to explain the "faint young Sun paradox," the distance between early Mars and the early Sun would also change as a function of solar mass; thus the luminosity to maintain liquid water on Mars would change as a function of solar mass. Assuming the eccentricity of the orbit of Mars and the angular momentum per unit mass of Mars remain constant with time, this lower boundary on luminosity is the red line in Figure 1(a).

Figure 1(b) contains luminosity *versus* time for the models from Guzik and Mussack (2010)'s mass-loss study and an additional early mass-loss model with a smaller initial mass (1.07 $M_\odot$). Models include two standard solar models with the GN93, AGS05 abundances, respectively, and early three mass-losing models using the AGS05 abundances and initial masses of 1.07, 1.15, and 1.30 $M_\odot$. The luminosity at early times is higher than the present solar luminosity for all early mass-loss models. The early mass-losing models asymptotically approach the standard solar models around 2 Gyrs. Using the luminosity and mass at
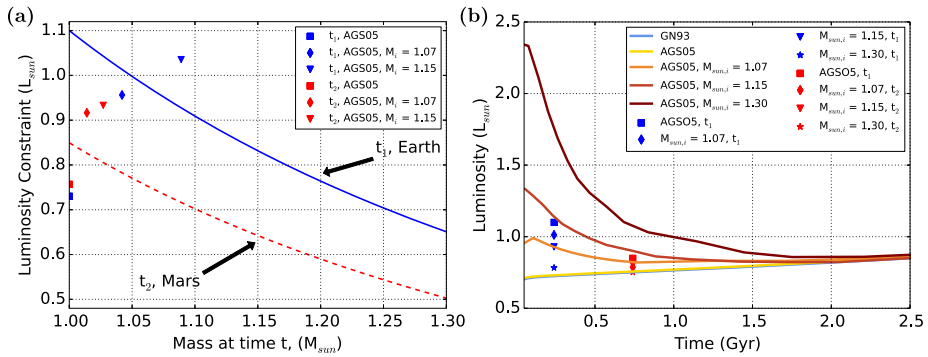
(a)

(b)

Figure 2 (**a**) Planetary constraints on luminosity as a function of solar mass at time (t). The values of mass and luminosity are plotted for the models with initial mass of 1.00 (*square*), 1.07 (*diamond*) and 1.15 (*triangle*) $M_\odot$ at $t = t_1$ (*blue*) and $t = t_2$ (*red*). (**b**) Zoom-in of luminosity *versus* time. With constraints on solar luminosity for the standard solar model (*square*), and mass-losing models with starting masses of 1.07 $M_\odot$ (*diamond*), 1.15 $M_\odot$ (*triangle*), and 1.30 $M_\odot$ (*star*).

t_1 and t_2 for each of the models in Figure 1(b), the constraints on solar luminosity can be compared to the models at these times (Figure 2).

Figure 2(a) compares the luminosity *versus* mass constraints described above to the mass and luminosity at times t_1 and t_2 for the standard solar model using the AGS05 abundances and models with initial masses of 1.07 and 1.15 $M_\odot$. As expected, the luminosity of the standard solar model at t_1 is lower than what is required to photodissociate water on Earth (blue square). Yet, this luminosity is also too low for there to even be liquid water on the surface of Earth at t_1 (Kasting, 2010). For the model with an initial mass of 1.07 $M_\odot$, luminosity remains low enough to keep liquid water on Earth (blue diamond), while water would photodissociate for the model with an initial mass of 1.15 $M_\odot$ (blue triangle). This rules out all models with a mass greater or equal to 1.15 $M_\odot$, with this mass-loss prescription. As expected, the luminosity of the standard solar model at t_2 would result in frozen and not liquid water on Mars (red square), while models with initial masses of 1.07 and 1.15 $M_\odot$ have a high enough luminosity at t_2 to allow for liquid water on Mars.

Figure 2(b) shows luminosity *versus* time for the models from Guzik and Mussack (2010)'s mass-loss study and an additional early mass-loss model with a lower initial mass (1.07 $M_\odot$), and the constraints derived for each of the models, given the mass at time t. The luminosity trace is greater than the symbol representing the constraint at that t_1 and mass for models with initial masses 1.15 and 1.30 $M_\odot$, meaning water would photodissociate from Earth for these models, while the luminosity trace is less than the symbol representing the constraint at that t_1 and mass for models with initial masses 1.00 and 1.07 $M_\odot$. Similarly, at t_2 the luminosity trace is less than the symbol representing the constraint at that t_2 for the standard solar model, meaning that water would be frozen on Mars, while the luminosity trace is greater than the symbol representing the constraint at that t_2 and mass for models with initial masses 1.07, 1.15, and 1.30 $M_\odot$.

Considering these constraints suggests that the initial mass of the Sun was less than 1.15 $M_\odot$ and greater than 1.00 $M_\odot$. Models with an initial mass of 1.30 $M_\odot$ have been ruled out by the constraints, but they are included in the remainder of the discussion to illustrate the tendency of the solar models with increasing initial mass. The exact mass limits would change based on the mass-loss treatment used in the solar evolution model; however, the constraints remain fixed given that the orbital eccentricities and angular momentum per

unit mass of the planet remain constant with time and changing solar mass. Because mass-loss rates in young solar-like stars remain an open question, with possible rates ranging between 1×10^{-12} $M_\odot$ yr^{-1} and 1×10^{-9} $M_\odot$ yr^{-1} (Caffe *et al.*, 1987; Gaidos, Güdel, and Blake, 2000; Wood *et al.*, 2002, 2005b,a; Cranmer, 2017; Fichtinger *et al.*, 2017), additional investigations, like the work of Minton and Malhotra (2007), examining how the initial-mass limit changes with different mass-loss treatments are worthwhile.

3.2. Impact of Mass Loss on Helioseismic Indicators

Here we extend the study of helioseismic predictions for mass-losing models conducted by Guzik and Mussack (2010) to include a model with a slightly lower initial mass. Figure 3(a) compares the inferred minus calculated sound speed for three mass-losing models to the inferred minus calculated sound speed for standard solar models using GN93 abundances and the AGS05 abundances. The mass-losing models incorporating the AGS05 abundances with initial masses of 1.07 $M_\odot$ (ML107), 1.15 $M_\odot$ (ML115), and 1.30 $M_\odot$ (ML130). The GN93, AGS05, ML115, and ML130 models were taken from Guzik and Mussack (2010).
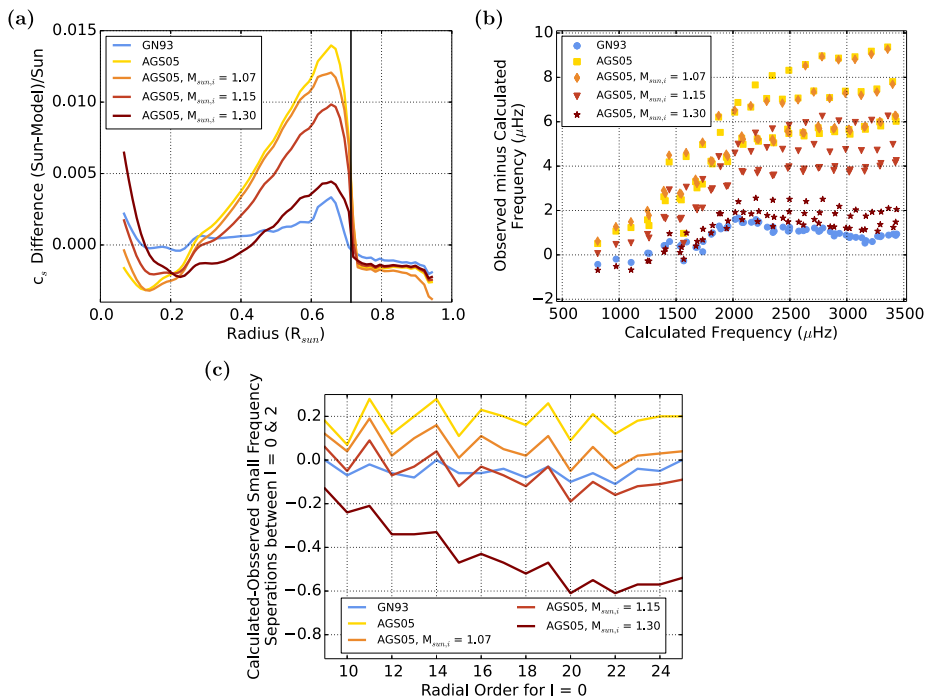

Figure 3 Comparison between helioseismic data and models. Models include standard solar models with GN93 (*blue*) and AGS05 (*yellow*) abundances and early mass-losing models using the AGS05 abundances and initial masses of 1.07, 1.15, and 1.30 $M_\odot$ (*orange to maroon*). The GN93, AGS05, mass-loss models with initial masses of 1.15 and 1.30 $M_\odot$ are from Guzik and Mussack (2010). (**a**) Differences between observed and calculated sound speed for calibrated solar models. The *black vertical line* at $R = 0.713$ $R_\odot$ marks the seismically inferred convection-zone base (Basu and Antia, 2004). (**b**) Differences between observed and calculated frequency *versus* calculated frequency. Modes $\ell = 0, 2, 10,$ and 20 are shown. The calculated frequencies were computed using the Pesnell (1990) non-adiabatic stellar pulsation code. The data were taken from Chaplin *et al.* (2007), Schou and Tomczyk (1996), García *et al.* (2001). (**c**) Calculated minus observed small separations for modes $\ell = 0$ and 2.

Table 2 Observed frequencies from LOWL instrument.

$\ell = 10$[a]			$\ell = 20$[a]		
n	Frequency (μHz)	Standard deviation (μHz)	n	Frequency (μHz)	Standard deviation (μHz)
6	1443.4270	0.0067	5	1566.5555	0.0110
7	1592.9194	0.0067	6	1734.1945	0.0085
8	1737.8435	0.0067	7	1893.9236	0.0120
9	1880.0386	0.0106	8	2050.0850	0.0120
10	2021.5305	0.0103	9	2203.1387	0.0131
11	2162.9443	0.0120	10	2352.4209	0.0124
12	2302.8081	0.0113	11	2498.9675	0.0120
13	2440.8206	0.0113	12	2644.8384	0.0113
14	2578.6360	0.0099	13	2790.6719	0.0103
15	2716.9546	0.0088	14	2935.9194	0.0106
16	2855.6741	0.0085	15	3080.4194	0.0106
17	2994.4666	0.0078	16	3224.3574	0.0131
18	3132.8979	0.0088	17	3368.0244	0.0173
19	3271.3110	0.0117			
20	3410.1030	0.0163			

[a]Data taken using the LOWL instrument (Tomczyk *et al.*, 1995) that can be found at Schou and Tomczyk (1996).

A vertical line marks the seismically inferred convection-zone base radius from Basu and Antia (2004) at $0.713 \pm 0.001\ R_\odot$. As the initial mass of the early mass-loss model increases, agreement between the inferred and calculated sound speeds improves within the radiative zone, below the base of the convection zone but above the core of the Sun. Agreement between the inferred and calculated sound speed is improved in the core of the Sun for the ML107 model, whereas agreement between the inferred and calculated sound speed in the core was decreased for the ML115 and ML130 models.

The observed minus calculated *versus* calculated non-adiabatic frequencies for modes of angular degree $\ell = 0$, 2, 10, and 20 are shown in Figure 3(b). These modes propagate into the solar interior below the convection zone. The calculated frequencies were computed using the Pesnell (1990) non-adiabatic stellar pulsation code. The data were taken from Chaplin *et al.* (2007), Schou and Tomczyk (1996) and García *et al.* (2001); the Schou and Tomczyk (1996) data were taken using the LOWL instrument (Tomczyk *et al.*, 1995) and can be found in Table 2. As the initial mass of the models increases, the differences between the observed and calculated frequency decrease. This suggests that in the region probed by modes of angular degree $\ell = 0$, 2, 10, and 20, a higher initial mass improves helioseismic agreement at the present time.

Figure 3(c) contains the small frequency separations of the standard models and the mass-losing models minus the solar-cycle frequency separations from the BiSON group (Chaplin *et al.*, 2007) for the $\ell = 0$ and 2 modes, which are sensitive to the structure of the core. Differences between calculated and observed small separations for $\ell = 0$ and 2 modes are decreased for mass-losing models with intermediate initial mass ($1.07 - 1.15\ M_\odot$), which interestingly have the same mass range relevant to the planetary constraints.

3.3. Combined Effects of Mass Loss and Dynamic Screening

Mussack and Däppen (2011) implemented a dynamic electron screening correction to a solar evolution model utilizing AGS05 abundances, and found improved agreement between the inferred and calculated sound speeds in the core of the Sun. As seen in Figure 3, early mass loss impacts the sounds speed and oscillation modes in the core of the Sun. Here we will investigate the combined effects of early mass-loss and a dynamic electron screening correction. It was expected that agreement between the inferred and the calculated sound speed will improve in both the core and the radiative zone for mass-losing models with dynamic screening corrections.

We explored different implementations of the dynamic electron screening correction. For the standard solar model using the AGS05 abundances (AGS05pp0, yellow dashed) and an early mass-loss model with an initial mass of 1.07 $M_\odot$ and the AGS05 abundances (ML107pp0, orange, dashed), the dynamic electron screening correction was implemented into the Iben evolution codes by simply removing the Salpeter (1954) screening enhancement, and treating all p–p reactions as unscreened reactions, because the reaction rate for unscreened and dynamically screened p–p reactions is about the same (Mussack and Däppen, 2011). To implement an approximate dynamic electron screening correction for the ML130rx0 model (maroon, dash-dot), an early mass-loss model with an initial mass of 1.30 $M_\odot$ using the AGS05 abundances, p–p, $^{12}C + p$, and $^{14}N + p$ reactions were treated as unscreened reactions by removing the Salpeter screening enhancement for these reactions; the CNO reactions, in particular $^{12}C + p$ and $^{14}N + p$, are important for higher initial-mass models and thus only implemented for this higher initial-mass model. While the 1.30 $M_\odot$ solar model was ruled out by luminosity constraints, the impact of dynamic screening in higher initial-mass stellar models remains as motivation for this implementation. The inclusion of the CNO reactions was done even though the molecular dynamics work was only completed for p–p reactions. The conditions used by Mao, Mussack, and Däppen (2009) and Mussack and Däppen (2011) are hotter and denser than the conditions in the core of the solar models, for the majority of the evolution (Figure 4). Figures 4(a) and 4(b) show the present day conditions for each of the solar models. Figures 4(c) and 4(d) display the density and temperature, respectively, of the innermost zone of the core as a function of time. The density only approaches the conditions used by Mao, Mussack, and Däppen (2009) and Mussack and Däppen (2011) at present time; only the model with an initial mass of 1.30 $M_\odot$ has a temperature near the conditions used by Mao, Mussack, and Däppen (2009) and Mussack and Däppen (2011) at a time other than present.

Figure 5 shows the inferred minus calculated sound speed for two standard solar models (solid line), three mass-losing models (solid line), and two mass-losing models with screening corrections (dashed line). The GN93, AGS05, ML107, and ML130 models are the models shown in Figure 3. All models except the GN93 (blue) standard solar model incorporate the AGS05 abundances (yellow to maroon). The dynamic screening correction approximation for only p–p reactions for the AGSpp0 and ML107pp0 models (dashed). The ML130rx0 model incorporates the dynamic screening correction approximation for the p–p reactions, as well as the $^{12}C + p$ and $^{14}N + p$ reactions of the CNO cycle (dash-dot). While the incorporation of the dynamic screening correction slightly improves agreement between the inferred and calculated sound speeds for the standard model (yellow, solid *vs.* dashed), the incorporation of the same approximation worsens agreement in the core and below the convection zone of Sun for the ML107pp0 model (orange, solid *vs.* dashed) (Figure 5). The implementation of the approximate dynamic screening correction for the ML130rx0 improves the sound-speed agreement in the core of the Sun as compared to the ML130 model,
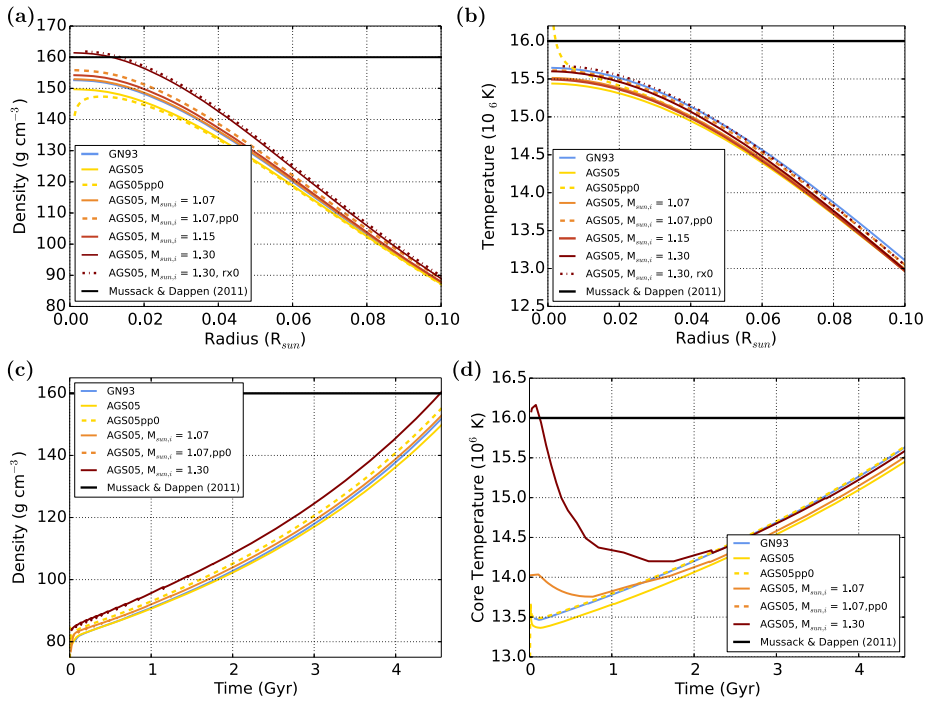
Figure 4 (**a**) Density and (**b**) temperature *versus* solar radius. Models include: standard solar models with GN93 (*blue*) and AGS05 (*yellow*) abundances, early mass-losing models using the AGS05 abundances and initial masses of 1.07 and 1.30 $M_\odot$ (orange and maroon), and early mass-loss models with dynamic screening at the present solar age using the AGS05 abundances and initial masses of 1.07 and 1.30 $M_\odot$ (*dashed lines of same color*). Conditions for electron screening approximation used by Mussack and Däppen ([2011](#)) are marked with a *thick black line*.

while it diminishes agreement with helioseismic data for the radiative zone above the core as compared to the ML130 model (Figure 5). The dynamic screening correction has a greater impact on the sound-speed agreement of the ML130rx0 model than the ML107pp0 model (Figure 5), which points to the need of a molecular dynamics study for CNO reactions.

The observed minus calculated *versus* calculated non-adiabatic frequencies for modes of angular degree $\ell = 0, 2, 10$, and 20, which propagate into the solar interior below the convection zone, are shown in Figure 6(a). The dynamic screening correction for the Ml107pp0 model slightly decreases agreement in the radiative zone as seen by the slight increase in observed minus calculated frequencies (Figure 6(a), orange). The dynamic screening correction for the ML130rx0 model decreases the agreement in the radiative zone compared to the ML130 model, as seen by increase in observed minus calculated frequencies (Figure 6(a), maroon). The dynamic screening correction has a greater effect on the observed minus calculated non-adiabatic frequencies for the ML130rx0 model than the ML107pp0 model (Figure 6(a) maroon and orange, respectively).

Figure 6(b) shows the small frequency separations of the models discussed above minus the observed small frequency separations from the BiSON group (Chaplin *et al.*, [2007](#)) for the $\ell = 0$ and 2 modes, which are sensitive to the structure of the core. While the decrease in sound-speed agreement in the core of the Sun for the ML107pp0 model compared to the ML107 model can be seen in the small frequency separations, which are sensitive to the
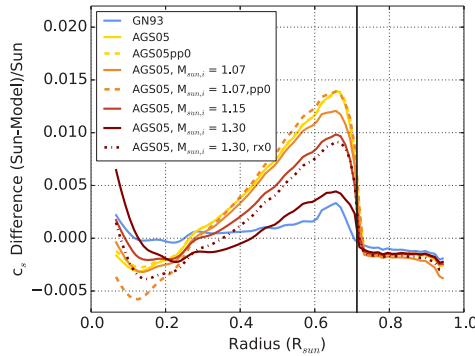
Figure 5 Relative difference between inferred and calculated sound speeds. Models include: standard solar models with GN93 and AGS05 abundances, a model with dynamic screening model correction for p–p reactions using the AGS05 abundances, early mass-losing models using the AGS05 abundances and initial masses of 1.07 and 1.30 $M_\odot$, and early mass-loss models with dynamic screening correction at the present solar age using the AGS05 abundances and initial masses of 1.07 and 1.30 $M_\odot$. For the model with an initial mass of 1.07 $M_\odot$, the screening correction is applied to p–p reactions. For the model with an initial mass of 1.30 $M_\odot$, the screening correction is applied to p–p reactions as well as ^{12}C + p and ^{14}N + p reactions.
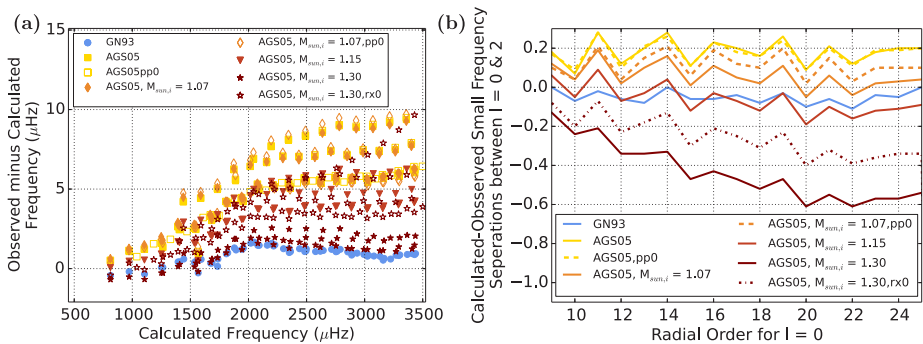

Figure 6 (**a**) Differences between observed and calculated frequency *versus* calculated frequency for modes $\ell = 0, 2, 10,$ and 20 modes. Models include: standard solar models with GN93 and AGS05 abundances, a dynamic screening model with correction for pp-reactions using the AGS05 abundances, early mass-losing models using the AGS05 abundances and initial masses of 1.07 and 1.30 $M_\odot$, and early mass-loss models with dynamic screening at the present solar age using the AGS05 abundances and initial masses of 1.07 and 1.30 $M_\odot$. The calculated frequencies were computed using the Pesnell (1990) non-adiabatic stellar pulsation code. The data are taken from Chaplin *et al.* (2007), Schou and Tomczyk (1996), and García *et al.* (2001). (**b**) Difference between calculated and observed small separations for modes $\ell = 0$ and 2. Models from the Guzik and Mussack (2010) models using the GN93 abundances and the AGS05 abundances and mass loss with initial mass of 1.07 $M_\odot$ and 1.30 $M_\odot$ are compared to the corresponding models with dynamic screening.

structure of the core, an improvement in sound-speed agreement in the core of the Sun for the ML130rx0 compared to the ML130 model can be seen in the small frequency separations (Figure 6(b) orange and maroon, respectively). The dynamic screening correction has a greater effect on small frequency separations for the $\ell = 0$ and 2 modes for the ML130rx0 model than the ML107pp0 model (Figure 6(b) maroon and orange).

Although the implementations of the dynamic screening correction approximation are different during the mass-loss phase of the ML107pp0 and ML130rx0 models, due to the

fact that the CNO cycle is important for the 1.30 $M_\odot$ model until enough mass is lost, the way that this correction affects agreement with helioseismic data is worthy of further investigation, especially in the light of the recent observation of gravity modes (Fossat *et al.*, 2017) which can be used to probe this region. Additionally, there is a need to extend the molecular dynamics dynamic electron screening study to other relevant pressures, temperature, and reactions.

4. Conclusion

Solar irradiance required to allow liquid water on early Earth and Mars was analyzed in the context of a more massive and luminous early Sun, where the initial solar mass ($M_{\odot,i}$) was determined to be $1.0 < M_{\odot,i} < 1.15\ M_\odot$ for a mass-loss model with an exponentially decaying mass-loss rate. Additionally, models with an initial mass between $1.07 - 1.15\ M_\odot$ correspond to better helioseismic agreement in both the core and the radiative zone as compared to the standard model. It is fair to conclude that models with an initial mass of 1.07 $M_\odot$ and an exponential mass-loss rate with an e-folding time of 1/10 of solar age fit both the constraints for early Earth and Mars; however, it is possible that models with a somewhat higher or lower $M_{\odot,i}$ are not ruled out by these constraints. The exact mass value will change with different abundances (*e.g.*, Asplund *et al.*, 2009) or with different mass-loss laws; the effects of these will be studied in future work.

In this paper, we approximate dynamic electron screening corrections by removing the Salpeter screening for specific reactions, particularly p–p, as well as $^{12}C + p$ and $^{14}N + p$ reactions for higher initial-mass stars. The small separations in the solar core are improved for both the intermediate mass and higher initial-mass models with specified dynamic screening corrections implementations, 1.07 and 1.30 $M_\odot$, respectively. Dynamic electron screening has significant effects and should be taken into account, but more molecular dynamics simulations are needed to derive and implement exact corrections.

Early mass loss is a promising avenue to help explain the presence of liquid water on early Mars and Earth, and also mitigate somewhat the solar abundance problem. But more work needs to be done to explore the consequences for solar Li depletion and solar core rotation (like that of Piau and Turck-Chièze, 2002; Turck-Chièze *et al.*, 2010) and to investigate early main-sequence mass-loss rates for solar analogs. Recent observations of g modes by Fossat *et al.* (2017) may provide key constraints on the evolution and structure of the solar core. Solar g-modes may provide a way to test and help constrain the initial solar mass and mass-loss history, and the dynamic screening implementations.

Disclosure of Potential Conflicts of Interest   The authors declare that they have no conflicts of interest.

References

Airapetian, V.S., Glocer, A., Gronoff, G., Hébrard, E., Danchi, W.: 2016, Prebiotic chemistry and atmospheric warming of early Earth by an active young Sun. *Nat. Geosci.* **9**, 452. DOI. ADS.

Allen, C.W.: 1973, *Astrophysical Quantities*. ADS.

Angulo, C., Arnould, M., Rayet, M., Descouvemont, P., Baye, D., Leclercq-Willain, C., Coc, A., Barhoumi, S., Aguer, P., Rolfs, C., Kunz, R., Hammer, J.W., Mayer, A., Paradellis, T., Kossionides, S., Chronidou, C., Spyrou, K., degl'Innocenti, S., Fiorentini, G., Ricci, B., Zavatarelli, S., Providencia, C., Wolters, H., Soares, J., Grama, C., Rahighi, J., Shotter, A., Lamehi Rachti, M.: 1999, A compilation of charged-particle induced thermonuclear reaction rates. *Nucl. Phys. B* **656**, 3. DOI. ADS.

Asplund, M., Grevesse, N., Sauval, A.J.: 2005, The solar chemical composition. In: Barnes, T.G. III, Bash, F.N. (eds.) *Cosmic Abundances as Records of Stellar Evolution and Nucleosynthesis*, *Astronomical Society of the Pacific Conference Series* **336**, 25. ADS.

Asplund, M., Grevesse, N., Sauval, A.J., Scott, P.: 2009, The chemical composition of the Sun. *Annu. Rev. Astron. Astrophys.* **47**, 481. DOI. ADS.

Basu, S., Antia, H.M.: 2004, Constraining solar abundances using helioseismology. *Astrophys. J. Lett.* **606**, L85. DOI. ADS.

Bibring, J.-P., Langevin, Y., Mustard, J.F., Poulet, F., Arvidson, R., Gendrin, A., Gondet, B., Mangold, N., Pinet, P., Forget, F., OMEGA Team, Berthé, M., Gomez, C., Jouglet, D., Soufflot, A., Vincendon, M., Combes, M., Drossart, P., Encrenaz, T., Fouchet, T., Merchiorri, R., Belluci, G., Altieri, F., Formisano, V., Capaccioni, F., Cerroni, P., Coradini, A., Fonti, S., Korablev, O., Kottsov, V., Ignatiev, N., Moroz, V., Titov, D., Zasova, L., Loiseau, D., Pinet, P., Doute, S., Schmitt, B., Sotin, C., Hauber, E., Hoffmann, H., Jaumann, R., Keller, U., Arvidson, R., Duxbury, T., Neukum, G.: 2006, Global mineralogical and aqueous Mars history derived from OMEGA/Mars express data. *Science* **312**, 400. DOI. ADS.

Boynton, W.V., Ming, D.W., Kounaves, S.P., Young, S.M.M., Arvidson, R.E., Hecht, M.H., Hoffman, J., Niles, P.B., Hamara, D.K., Quinn, R.C., Smith, P.H., Sutter, B., Catling, D.C., Morris, R.V.: 2009, Evidence for calcium carbonate at the mars phoenix landing site. *Science* **325**(5936), 61. DOI.

Bristow, T.F., Haberle, R.M., Blake, D.F., Des Marais, D.J., Eigenbrode, J.L., Fairén, A.G., Grotzinger, J.P., Stack, K.M., Mischna, M.A., Rampe, E.B., Siebach, K.L., Sutter, B., Vaniman, D.T., Vasavada, A.R.: 2017, Low Hesperian PCO2 constrained from in situ mineralogical analysis at Gale Crater, Mars. *Proc. Natl. Acad. Sci. USA* **114**, 2166. DOI. ADS.

Caffe, M.W., Hohenberg, C.M., Swindle, T.D., Goswami, J.N.: 1987, Evidence in meteorites for an active early sun. *Astrophys. J. Lett.* **313**, L31. DOI. ADS.

Carr, M.H.: 1996, *Water on Mars*, Oxford Univ. Press, New York. ADS.

Chaplin, W.J., Serenelli, A.M., Basu, S., Elsworth, Y., New, R., Verner, G.A.: 2007, Solar heavy-element abundance: Constraints from frequency separation ratios of low-degree p-modes. *Astrophys. J.* **670**, 872. DOI. ADS.

Charnay, B., Le Hir, G., Fluteau, F., Forget, F., Catling, D.C.: 2017, A warm or a cold early Earth? New insights from a 3-D climate-carbon model. *Earth Planet. Sci. Lett.* **474**, 97. DOI. ADS.

Cohen, E.R., Taylor, B.N.: 1988, The 1986 CODATA recommended values of the fundamental physical constants. *J. Phys. Chem. Ref. Data* **17**, 1795. DOI. ADS.

Cox, A.N., Guzik, J.A., Kidman, R.B.: 1989, Oscillations of solar models with internal element diffusion. *Astrophys. J.* **342**, 1187. DOI. ADS.

Cranmer, S.R.: 2017, Mass-loss rates from coronal mass ejections: A predictive theoretical model for solar-type stars. *Astrophys. J.* **840**, 114. DOI. ADS.

Ehlmann, B.L., Mustard, J.F., Murchie, S.L., Poulet, F., Bishop, J.L., Brown, A.J., Calvin, W.M., Clark, R.N., Des Marais, D.J., Milliken, R.E., Roach, L.H., Roush, T.L., Swayze, G.A., Wray, J.J.: 2008, Orbital identification of carbonate-bearing rocks on Mars. *Science* **322**, 1828. DOI. ADS.

Ehlmann, B.L., Mustard, J.F., Murchie, S.L., Bibring, J.-P., Meunier, A., Fraeman, A.A., Langevin, Y.: 2011, Subsurface water and clay mineral formation during the early history of Mars. *Nature* **479**, 53. DOI. ADS.

Feldman, W.C., Asbridge, J.R., Bame, S.J., Gosling, J.T.: 1977, Plasma and magnetic fields from the Sun. In: White, O.R. (ed.) *The Solar Output and Its Variation*, 351, Colorado Assoc. Univ. Press, Boulder. ADS.

Ferguson, J.W., Alexander, D.R., Allard, F., Barman, T., Bodnarik, J.G., Hauschildt, P.H., Heffner-Wong, A., Tamanai, A.: 2005, Low-temperature opacities. *Astrophys. J.* **623**, 585. DOI. ADS.

Fichtinger, B., Güdel, M., Mutel, R.L., Hallinan, G., Gaidos, E., Skinner, S.L., Lynch, C., Gayley, K.G.: 2017, Radio emission and mass loss rate limits of four young solar-type stars. *Astron. Astrophys.* **599**, A127. DOI. ADS.

Forget, F., Wordsworth, R., Millour, E., Madeleine, J.-B., Kerber, L., Leconte, J., Marcq, E., Haberle, R.M.: 2013, 3D modelling of the early martian climate under a denser CO_2 atmosphere: Temperatures and CO_2 ice clouds. *Icarus* **222**, 81. DOI. ADS.

Formicola, A., Imbriani, G., Costantini, H., Angulo, C., Bemmerer, D., Bonetti, R., Broggini, C., Corvisiero, P., Cruz, J., Descouvemont, P., Fülöp, Z., Gervino, G., Guglielmetti, A., Gustavino, C., Gyürky, G., Jesus, A.P., Junker, M., Lemut, A., Menegazzo, R., Prati, P., Roca, V., Rolfs, C., Romano, M., Rossi Al-

varez, C., Schümann, F., Somorjai, E., Straniero, O., Strieder, F., Terrasi, F., Trautvetter, H.P., Vomiero, A., Zavatarelli, S.: 2004, Astrophysical S-factor of ^{14}N(p,γ)^{15}O. *Phys. Lett. B* **591**, 61. DOI. ADS.

Fossat, E., Boumier, P., Corbard, T., Provost, J., Salabert, D., Schmider, F.X., Gabriel, A.H., Grec, G., Renaud, C., Robillot, J.M., Roca-Cortés, T., Turck-Chièze, S., Ulrich, R.K., Lazrek, M.: 2017, Asymptotic g-modes: Evidence for a rapid rotation of the solar core. *Astron. Astrophys.* **604**, A40. DOI. ADS.

Gaidos, E.J., Güdel, M., Blake, G.A.: 2000, The Faint Young Sun Paradox: An observational test of an alternative solar model. *Geophys. Res. Lett.* **27**, 501. DOI. ADS.

Gallet, F., Bouvier, J.: 2013, Improved angular momentum evolution model for solar-like stars. *Astron. Astrophys.* **556**, A36. DOI. ADS.

García, R.A., Régulo, C., Turck-Chièze, S., Bertello, L., Kosovichev, A.G., Brun, A.S., Couvidat, S., Henney, C.J., Lazrek, M., Ulrich, R.K., Varadi, F.: 2001, Low-degree low-order solar p modes as seen by GOLF On board SOHO. *Solar Phys.* **200**, 361. DOI. ADS.

Gendrin, A., Mangold, N., Bibring, J.-P., Langevin, Y., Gondet, B., Poulet, F., Bonello, G., Quantin, C., Mustard, J., Arvidson, R., Le Mouélic, S.: 2005, Sulfates in martian layered terrains: The OMEGA/Mars express view. *Science* **307**, 1587. DOI. ADS.

Grevesse, N., Noels, A.: 1993, Cosmic abundances of the elements. In: Prantzos, N., Vangioni-Flam, E., Casse, M. (eds.) *Origin and Evolution of the Elements*, 15. ADS.

Guenther, D.B., Demarque, P., Kim, Y.-C., Pinsonneault, M.H.: 1992, Standard solar model. *Astrophys. J.* **387**, 372. DOI. ADS.

Guzik, J.A., Mussack, K.: 2010, Exploring mass loss, low-Z accretion, and convective overshoot in solar models to mitigate the solar abundance problem. *Astrophys. J.* **713**, 1108. DOI. ADS.

Guzik, J.A., Swenson, F.J.: 1997, Seismological comparisons of solar models with element diffusion using the MHD, Opal, and Sireff equations of state. *Astrophys. J.* **491**, 967. DOI. ADS.

Guzik, J.A., Watson, L.S., Cox, A.N.: 2005, Can enhanced diffusion improve helioseismic agreement for solar models with revised abundances? *Astrophys. J.* **627**, 1049. DOI. ADS.

Guzik, J.A., Willson, L.A., Brunish, W.M.: 1987, A comparison between mass-losing and standard solar models. *Astrophys. J.* **319**, 957. DOI. ADS.

Iben, I. Jr.: 1963, A comparison between homogeneous stellar models and the observations. *Astrophys. J.* **138**, 452. DOI. ADS.

Iben, I. Jr.: 1965a, Stellar evolution, I: The approach to the main sequence. *Astrophys. J.* **141**, 993. DOI. ADS.

Iben, I. Jr.: 1965b, Stellar evolution, II: The evolution of a 3 M_{sun} star from the main sequence through core helium burning. *Astrophys. J.* **142**, 1447. DOI. ADS.

Iglesias, C.A., Rogers, F.J.: 1996, Updated opal opacities. *Astrophys. J.* **464**, 943. DOI. ADS.

Kasting, J.F.: 1988, Runaway and moist greenhouse atmospheres and the evolution of Earth and Venus. *Icarus* **74**, 472. DOI. ADS.

Kasting, J.F.: 1991, CO2 condensation and the climate of early Mars. *Icarus* **94**, 1. DOI. ADS.

Kasting, J.F.: 2010, Early Earth: Faint young Sun redux. *Nature* **464**, 687. DOI. ADS.

Kasting, J.F., Whitmire, D.P., Reynolds, R.T.: 1993, Habitable zones around main sequence stars. *Icarus* **101**, 108. DOI. ADS.

Lanza, N.L., Wiens, R.C., Arvidson, R.E., Clark, B.C., Fischer, W.W., Gellert, R., Grotzinger, J.P., Hurowitz, J.A., McLennan, S.M., Morris, R.V., Rice, M.S., Bell, J.F., Berger, J.A., Blaney, D.L., Bridges, N.T., Calef, F., Campbell, J.L., Clegg, S.M., Cousin, A., Edgett, K.S., Fabre, C., Fisk, M.R., Forni, O., Frydenvang, J., Hardy, K.R., Hardgrove, C., Johnson, J.R., Lasue, J., Le Mouélic, S., Malin, M.C., Mangold, N., Martın-Torres, J., Maurice, S., McBride, M.J., Ming, D.W., Newsom, H.E., Ollila, A.M., Sautter, V., Schröder, S., Thompson, L.M., Treiman, A.H., VanBommel, S., Vaniman, D.T., Zorzano, M.-P.: 2016, Oxidation of manganese in an ancient aquifer, Kimberley formation, Gale crater, Mars. *Geophys. Res. Lett.* **43**, 7398. DOI. ADS.

Malin, M.C., Edgett, K.S.: 2000, Evidence for recent groundwater seepage and surface runoff on Mars. *Science* **288**, 2330. DOI. ADS.

Malin, M.C., Edgett, K.S.: 2003, Evidence for persistent flow and aqueous sedimentation on early Mars. *Science* **302**, 1931. DOI. ADS.

Mao, D., Mussack, K., Däppen, W.: 2009, Dynamic screening in solar plasma. *Astrophys. J.* **701**, 1204. DOI. ADS.

Minton, D.A., Malhotra, R.: 2007, Assessing the massive young sun hypothesis to solve the warm young earth puzzle. *Astrophys. J.* **660**, 1700. DOI. ADS.

Mojzsis, S.J., Harrison, T.M., Pidgeon, R.T.: 2001, Oxygen-isotope evidence from ancient zircons for liquid water at the Earth's surface 4,300 Myr ago. *Nature* **409**, 178. ADS.

Morris, R.V., Ruff, S.W., Gellert, R., Ming, D.W., Arvidson, R.E., Clark, B.C., Golden, D.C., Siebach, K., Klingelhöfer, G., Schröder, C., Fleischer, I., Yen, A.S., Squyres, S.W.: 2010, Identification of carbonate-rich outcrops on Mars by the spirit rover. *Science* **329**, 421. DOI. ADS.

Mussack, K., Däppen, W.: 2011, Dynamic screening correction for solar p–p reaction rates. *Astrophys. J.* **729**, 96. DOI. ADS.

Osterloo, M.M., Hamilton, V.E., Bandfield, J.L., Glotch, T.D., Baldridge, A.M., Christensen, P.R., Tornabene, L.L., Anderson, F.S.: 2008, Chloride-bearing materials in the southern highlands of Mars. *Science* **319**, 1651. DOI. ADS.

Pesnell, W.D.: 1990, Nonradial, nonadiabatic stellar pulsations. *Astrophys. J.* **363**, 227. DOI. ADS.

Piau, L., Turck-Chièze, S.: 2002, Lithium depletion in pre-main-sequence solar-like stars. *Astrophys. J.* **566**, 419. DOI. ADS.

Poulet, F., Bibring, J.-P., Mustard, J.F., Gendrin, A., Mangold, N., Langevin, Y., Arvidson, R.E., Gondet, B., Gomez, C.: 2005, Phyllosilicates on Mars and implications for early martian climate. *Nature* **438**, 623. DOI. ADS.

Ribas, I.: 2010, The Sun and stars as the primary energy input in planetary atmospheres. In: Kosovichev, A.G., Andrei, A.H., Rozelot, J.-P. (eds.) *Solar and Stellar Variability: Impact on Earth and Planets*, *IAU Symp.* **264**, 3. DOI. ADS.

Sackmann, I.-J., Boothroyd, A.I.: 2003, Our Sun, V: A bright young sun consistent with helioseismology and warm temperatures on ancient Earth and Mars. *Astrophys. J.* **583**, 1024. DOI. ADS.

Salpeter, E.E.: 1954, Electrons screening and thermonuclear reactions. *Aust. J. Phys.* **7**, 373. DOI. ADS.

Schatzman, E.: 1962, A theory of the role of magnetic activity during star formation. *Ann. Astrophys.* **25**, 18. ADS.

Schou, J., Tomczyk, S.: 1996, m2 table. http://www.hao.ucar.edu/public/research/mlso/LowL/data.html.

Squyres, S.W., Grotzinger, J.P., Arvidson, R.E., Bell, J.F., Calvin, W., Christensen, P.R., Clark, B.C., Crisp, J.A., Farrand, W.H., Herkenhoff, K.E., Johnson, J.R., Klingelhöfer, G., Knoll, A.H., McLennan, S.M., McSween, H.Y., Morris, R.V., Rice, J.W., Rieder, R., Soderblom, L.A.: 2004, *In situ* evidence for an ancient aqueous environment at meridiani planum, Mars. *Science* **306**, 1709. DOI. ADS.

Squyres, S.W., Arvidson, R.E., Ruff, S., Gellert, R., Morris, R.V., Ming, D.W., Crumpler, L., Farmer, J.D., Des Marais, D.J., Yen, A., McLennan, S.M., Calvin, W., Bell, J.F., Clark, B.C., Wang, A., McCoy, T.J., Schmidt, M.E., de Souza, P.A.: 2008, Detection of silica-rich deposits on Mars. *Science* **320**, 1063. DOI. ADS.

Tomczyk, S., Streander, K., Card, G., Elmore, D., Hull, H., Cacciani, A.: 1995, An instrument to observe low-degree solar oscillations. *Solar Phys.* **159**, 1. DOI. ADS.

Turbet, M., Forget, F., Head, J.W., Wordsworth, R.: 2017, 3D modelling of the climatic impact of outflow channel formation events on early Mars. *Icarus* **288**, 10. DOI. ADS.

Turck-Chieze, S., Daeppen, W., Casse, M.: 1988, High mass loss in the young Sun. In: Rolfe, E.J. (ed.) *Seismology of the Sun and sun-like stars*, *ESA Special Publication* **286**. ADS.

Turck-Chièze, S., Piau, L., Couvidat, S.: 2011, The solar energetic balance revisited by young solar analogs, helioseismology, and neutrinos. *Astrophys. J. Lett.* **731**, L29. DOI. ADS.

Turck-Chièze, S., Palacios, A., Marques, J.P., Nghiem, P.A.P.: 2010, Seismic and dynamical solar models, I: The impact of the solar rotation history on neutrinos and seismic indicators. *Astrophys. J.* **715**, 1539. DOI. ADS.

Weber, E.J., Davis, L. Jr.: 1967, The angular momentum of the solar wind. *Astrophys. J.* **148**, 217. DOI. ADS.

Weiss, A., Heners, N.: 2013, Low-mass stars: Open problems all along their evolution. *Eur. Phys. J. Web Conf.* **43**, 01002. DOI. ADS.

Whitmire, D.P., Doyle, L.R., Reynolds, R.T., Matese, J.J.: 1995, A slightly more massive young Sun as an explanation for warm temperatures on early Mars. *J. Geophys. Res.* **100**, 5457. DOI. ADS.

Willson, R.C., Hudson, H.S., Frohlich, C., Brusa, R.W.: 1986, Long-term downward trend in total solar irradiance. *Science* **234**, 1114. DOI. ADS.

Wolff, S., Simon, T.: 1997, The angular momentum of main sequence stars and its relation to stellar activity. *Publ. Astron. Soc. Pac.* **109**, 759. DOI. ADS.

Wood, B.E., Müller, H.-R., Zank, G.P., Linsky, J.L.: 2002, Measured mass-loss rates of solar-like stars as a function of age and activity. *Astrophys. J.* **574**, 412. DOI. ADS.

Wood, B.E., Müller, H.-R., Zank, G.P., Linsky, J.L., Redfield, S.: 2005a, New mass-loss measurements from astrospheric Lyα absorption. *Astrophys. J. Lett.* **628**, L143. DOI. ADS.

Wood, B.E., Redfield, S., Linsky, J.L., Müller, H.-R., Zank, G.P.: 2005b, Stellar Lyα emission lines in the Hubble space telescope archive: Intrinsic line fluxes and absorption from the heliosphere and astrospheres. *Astrophys. J. Suppl.* **159**, 118. DOI. ADS.

Wordsworth, R.D.: 2016, The climate of early Mars. *Annu. Rev. Earth Planet. Sci.* **44**, 381. DOI. ADS.